

Numerical Heat Transfer, Part A: Applications

An International Journal of Computation and Methodology

ISSN: 1040-7782 (Print) 1521-0634 (Online) Journal homepage: <http://www.tandfonline.com/loi/unht20>

Numerical predictions of the effective thermal conductivity for needed C/C-SiC composite materials

Wen-Zhen Fang, Jian-Jun Gou, Hu Zhang, Qinjun Kang & Wen-Quan Tao

To cite this article: Wen-Zhen Fang, Jian-Jun Gou, Hu Zhang, Qinjun Kang & Wen-Quan Tao (2016) Numerical predictions of the effective thermal conductivity for needed C/C-SiC composite materials, Numerical Heat Transfer, Part A: Applications, 70:10, 1101-1117, DOI: [10.1080/10407782.2016.1230427](https://doi.org/10.1080/10407782.2016.1230427)

To link to this article: <https://doi.org/10.1080/10407782.2016.1230427>



Published online: 24 Oct 2016.



Submit your article to this journal [↗](#)



Article views: 120



View related articles [↗](#)



View Crossmark data [↗](#)



Citing articles: 5 View citing articles [↗](#)

Numerical predictions of the effective thermal conductivity for needled C/C-SiC composite materials

Wen-Zhen Fang^a, Jian-Jun Gou^a, Hu Zhang^a, Qinjun Kang^b, and Wen-Quan Tao^a

^aKey Laboratory of Thermo-Fluid Science and Engineering, MOE, Xi'an Jiaotong University, Xi'an, China;

^bComputational Earth Science Group (EES-16), Los Alamos National Laboratory, Los Alamos, NM, USA

ABSTRACT

In the present paper, the complicated structures of needled C/C-SiC composite materials with random distributions of fibers and pores are reconstructed. A multiple-relaxation-time (MRT) lattice Boltzmann model with off-diagonal elements in the relaxation time matrix is adopted to predict longitudinal and transverse thermal conductivities of needled C/C-SiC composite materials whose constituents are anisotropic. The accuracy of the proposed method is verified by the good agreements between the numerical results and experimental data obtained by the Hot Disk thermal constants analyzer. After validations, the factors that influence the effective thermal conductivities of the composite materials are investigated.

ARTICLE HISTORY

Received 2 April 2016

Accepted 9 August 2016

1. Introduction

Carbon fiber reinforced carbon and silicon carbide dual matrix composite materials (C/C-SiC) have received considerable attention for applications in the spacecraft thermal protection system due to their low density and high strength. Compared with the carbon/carbon composite materials (C/C), the C/C-SiC composite materials have higher oxidation resistance and a more stable friction coefficient [1–3]. The needle fiber bundles improve the interlaminar shear strength, and therefore the needled C/C-SiC composite materials have the potential to be used as spacecraft braking materials. The mechanical strength, thermal expansion coefficient, and friction coefficient of the needled C/C-SiC composite materials have been greatly investigated [4–8]. Although thermal conductivity is a very important parameter to quantitatively describe the heat transfer capacity of materials when they serve as braking materials, little research has been conducted on determining the effective thermal conductivity of the needled C/C-SiC composite materials, especially by numerical predictions. Following is a brief review on the experimental studies in this regard. Chen et al. [9] adopted a laser apparatus to measure the thermal diffusivity of the needled C/SiC-TaC composite materials with different TaC contents; Cheng et al. [10] also used a laser apparatus to determine the longitudinal and transverse thermal diffusivities of three-dimensional C/SiC materials from the ambient temperature to 1,400°C, and then fitted them by a multinomial function; Cai et al. [5] applied the isotropic module of the Hot Disk thermal constants analyzer based on the transient plane source method to measure the effective thermal conductivity of needled C/C-SiC composite materials, but the feasibility of such isotropic treatment is questionable because the thermal properties of needled C/C-SiC composite materials along the longitudinal and transverse directions are quite different. The experimental methods to determine the thermophysical properties, including effective thermal conductivity, are very important; however, it is time-consuming and resource-intensive. In this regard, numerical

CONTACT Wen-Quan Tao  wqtao@mail.xjtu.edu.cn  Key Laboratory of Thermo-Fluid Science and Engineering, MOE, Xi'an Jiaotong University, Xi'an 710049, China.

Color versions of one or more of the figures in the article can be found online at www.tandfonline.com/unht.

© 2016 Taylor & Francis

NOMENCLATURE

c	pseudo sound speed, m/s	ϕ	volume fraction
T	temperature, K	λ	thermal conductivity, W/(m · K)
$c_p, \rho c_p$	heat capacity, J/(kg · K), volumetric heat capacity, J/(m ³ · K)	τ	relaxation time coefficient
D	thermal diffusivity, m ² /s	Subscript	
e	discrete velocity	α	direction of the temperature distribution function
f, f^{eq}	temperature distribution function, equivalent distribution function	$\bar{\alpha}$	directions opposite to α
m, M	moment vector, transformation matrix	c, w	nonwoven cloth, short-cut fiber web
q, T	heat flux, W/m ² , temperature, K	e	effective
S	relaxation time matrix	i, j	number index
$t, \delta t, \delta x$	time, time step, space step	L	longitudinal
Ω	collision matrix	T	transverse
ε, γ	constants, $\varepsilon = 2\gamma$, and $\gamma = 1/8$	x, y, z	direction index
δ	thicknesses of materials, m	η, ζ	principle axis of heat conduction

simulation provides an alternative and efficient way. And once the numerical model is validated, it is quite easy to investigate the influences of different factors by numerical simulation. In addition, the numerical predictions of the thermophysical properties of the composite materials can provide the guideline for improving the designing of the structure of the composite materials to meet engineering requirements.

Now, a question may arise as to why so far we could not find a numerical study (at least to the authors' knowledge) of predicting the effective thermal conductivities of needled C/C-SiC composite materials. To our understanding, there are two major challenges for numerically predicting the effective thermal conductivities of needled C/C-SiC composite materials. One is how to deal with the very complicated structure of the composite materials with random distributions of pores and fibers. The other challenge is how to deal with the anisotropic heat transfer problem due to the anisotropic fibers with different thermal conductivities in the axial and radial directions contained in the composite materials. The commercial software is an efficient numerical tool to determine the effective thermal conductivity of the composite materials [11], but it cannot read or reconstruct the complicated structure of the composite materials with randomly distributed pores and fibers. The self-programming codes can reconstruct a stochastic geometry structure; however, the code development based on the original lattice Boltzmann method (LBM) [12–14] or traditional finite volume method [15,16] to solve the anisotropic heat transfer is not straightforward. The LBM has an advantage over the finite volume method in programming and dealing with internal boundary conditions. Recently, the original LBM has been adopted to numerically predict the effective thermal conductivities of granular materials [17], netlike-structure materials [18], and fibrous materials [19]. However, they are all based on the assumption that the thermal conductivities of the constituent materials of the composite materials are all isotropic. It is because the original LB model, the BGK model [20], with single relaxation time does not have enough parameters to fully consider the anisotropic heat conduction problem. In recent years, the multiple-relaxation-time (MRT) LB model has been developed to solve the fluid flow and heat transfer problem due to its advantage of higher stability and accuracy over the original LBM [21]. The MRT LB model with a relaxation time matrix has sufficient parameters to fully describe the anisotropic diffusion problem [22]. In the previous MRT LB model, the relaxation time matrix of the MRT LB model is diagonal, and has no ability to consider the anisotropic heat conduction problem [23]. Yoshida and Nagoka [24] proposed an MRT LB model with off-diagonal elements in the relaxation time matrix to simulate the anisotropic advection-diffusion problem in the homogeneous medium. In the present paper, an MRT LB model with off-diagonal elements in the relaxation time matrix is developed to numerically predict the effective thermal conductivity of the heterogeneous materials whose constituent materials can be anisotropic, like needled C/C-SiC composites materials. To validate the feasibility and accuracy of the method proposed in the present

paper, some corresponding experimental measurements based on the Hot Disk method are conducted to measure the heat capacity of the composite materials and then to determine the longitudinal and transverse thermal conductivities of the needled C/C-SiC composite materials. The Hot Disk thermal constants analyzer based on the transient plane source method can determine the longitudinal and transverse thermal conductivities of the needled C/C-SiC composite materials simultaneously [25]. After validations, the influences of needle fiber bundles, porosity, carbon matrix contents, fiber volume fractions of the composite materials, and thermal conductivity of fibers and internal thermal contact resistance on the effective thermal conductivity are investigated.

In the present paper, the numerical method to predict the effective thermal conductivities of the needled C/C-SiC composite materials is presented. The rest of the paper is organized as follows. In Section 2, the developed numerical method is introduced in details, including the reconstruction of the microstructure, the MRT LBM, and how to use it to predict the effective thermal conductivity of C/C-SiC. In Section 3, the experimental method to determine the anisotropic thermal conductivities via Hot Disk is briefly provided. Section 4 gives detailed presentation of the numerical results, including discussion on the effects of a number of factors. Finally, some conclusions are drawn in Section 5.

2. Numerical method

2.1. Microstructure of the composite materials and their reconstruction

Different processing techniques for manufacturing needled C/C-SiC composite materials have been reported in the literature [3–5]. In general, the preform of the needled C/C-SiC composite materials is made by repeatedly overlapping layers of 0° nonwoven cloth, short-cut fiber wet, and 90° nonwoven cloth to form an elementary layer, and then needling a number of elementary layers together (see Figure 1). The needled C/C-SiC composite material is prepared by two steps. The first step is to make the porous C/C composite material by chemical vapor infiltration or polymer impregnation pyrolysis process. The second step is the liquid silicon infiltration process to form the final C/C-SiC composite material [5, 8]. If we assume that no any residual Si exists in the composite materials, the constituents of the needled C/C-SiC composite material include the carbon fiber (T300), the carbon matrix, the SiC matrix, and the pore. The diameter of the T300 carbon fiber is $6.9\ \mu\text{m}$ [26]. The overall and side-view pictures of the needled C/C-SiC composite material are shown in Figure 2a. The scanning electron microscope pictures of the nonwoven cloth, the short-cut fiber web, and the needle fiber

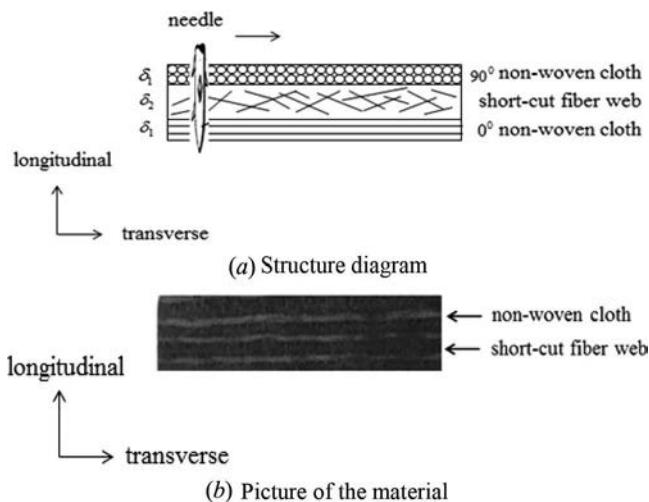


Figure 1. Structure of the needled C/C-SiC composite material.

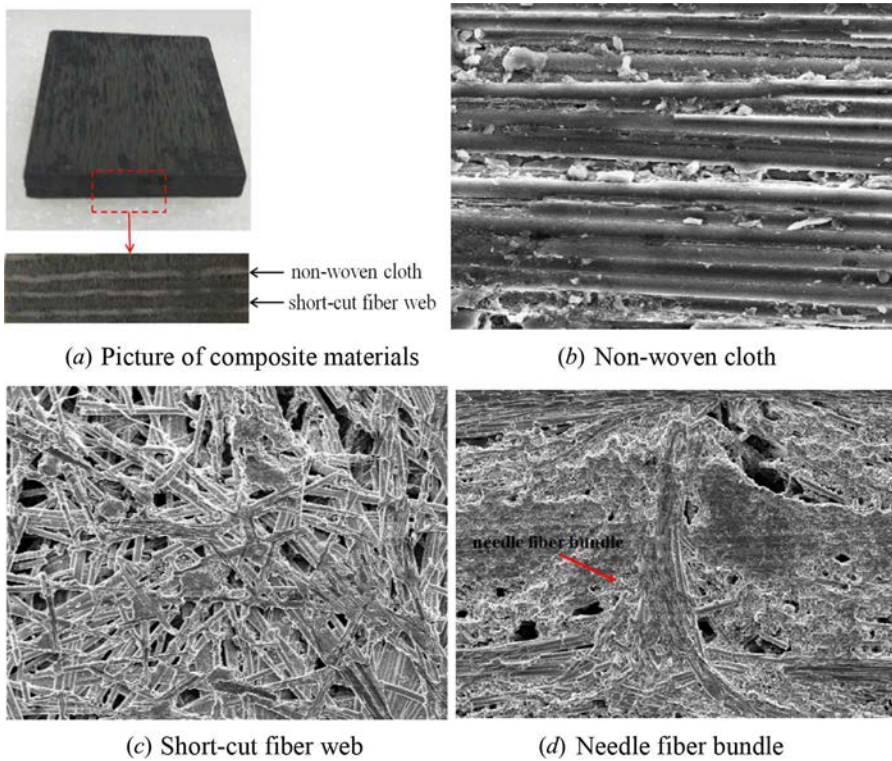


Figure 2. Scanning electron microscope pictures.

bundles are shown in [Figures 2b–2d](#), respectively. From those pictures, we can see that all fibers in the nonwoven cloth are compactly arranged in one direction, and only a few isolated pores exist in the matrix during the infiltration process. However, in the short-cut fiber web, the short-cut fibers are sparsely and randomly dispersed in the plane, and there are much more isolated pores than those in the nonwoven cloth. During the production procedures, the silicon infiltrates the C/C composite materials through the pores and then it reacts with the carbon matrix to form SiC. After infiltration, some isolated pores remain. Therefore, in our model, the carbon matrix is treated as a continuous phase while the SiC matrix and the pore are dealt with as disperse phases.

The stochastic structure of materials should be reconstructed first if we use the MRT LBM to numerically predict the effective thermal conductivity of the heterogeneous materials. [Figures 3a–3c](#) show the reconstructed unit cell structures of the short-cut fiber web, nonwoven cloth, and needle fiber bundle, respectively. For the short-cut fiber web, the reconstruction methods are described as follows. First, the randomly distributed fibers are regenerated by a computation code. When one fiber grows to reach a certain length or touch the boundary wall of the unit cell, it stops growing; and when the fiber fraction of fibers reaches a specified value, the regeneration of the fiber is completed. Second, the phases of the SiC matrix and pores are regenerated following the procedures of the QSGS method proposed by Wang et al. [17]. Finally, the grid cells not occupied by any phases of the fibers, the SiC matrix, and the pores are the carbon matrix. [Figure 3b](#) shows the diagram of the ideal structure of the nonwoven cloth and its reconstruction unit cell structure. To reduce the calculation regions, we selected a single fiber with dual matrices (C and SiC) and pores as the unit cell of the nonwoven cloth. As for the needle fiber bundle, the diagram of the simplified structure and its reconstruction unit cell structures are shown in [Figure 3c](#). Here, we assume that the needle fibers are unidirectional. Based on the reconstructed unit cell structures of the nonwoven cloth, short-cut fiber web, and needle fiber bundle, we can adopt the MRT LBM to numerically determine their thermal conductivities,

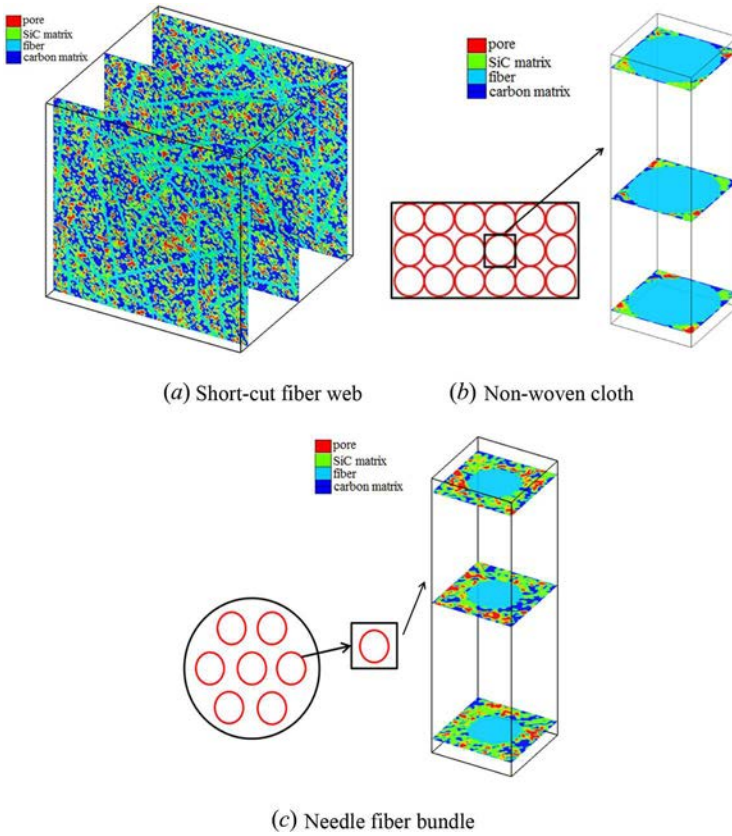


Figure 3. Reconstructed unit cell structures.

respectively, and then calculate the total thermal conductivity of the needed C/C-SiC composite materials (see Section 2.3). The details will be described in the following sections.

2.2. MRT LB model

Taking the two-phase composite materials as an example, the energy transport equations for anisotropic heat conduction in heterogeneous materials without any heat sources can be expressed as

$$\frac{\partial T_A}{\partial t} = \frac{\partial}{\partial x_i} \left((D_{ij})_A \frac{\partial T_A}{\partial x_j} \right) \quad (1)$$

$$\frac{\partial T_B}{\partial t} = \frac{\partial}{\partial x_i} \left((D_{ij})_B \frac{\partial T_B}{\partial x_j} \right) \quad (2)$$

where the subscripts A and B represent two different components, T is the temperature, and D_{ij} is the thermal diffusivity matrix. The conditions at the interfaces between the two different components must satisfy the continuities of temperature and heat flux [27]:

$$T_A = T_B \quad (3)$$

$$-n_i (\lambda_{ij})_A \frac{\partial T_A}{\partial x_j} = -n_i (\lambda_{ij})_B \frac{\partial T_B}{\partial x_j} \quad (4)$$

where λ_{ij} denotes the thermal conductivity matrix, and n_i is the unit normal vector at the interfaces.

LBM is an alternative approach to solve the energy transport equations based on the evolution of the discrete particle distribution function. The relaxation time of the LB equation corresponds to the thermal diffusivity of the materials. Thus, an LB model with multiple relaxation times is required for the anisotropic heat transfer problem. In the present paper, the D3Q7 MRT LBM is adopted (Figure 4). The evolution of the discrete particle distribution function of the MRT LB model for each component of the heterogeneous materials can both be generally described by [12]

$$\mathbf{f}(\mathbf{x} + \mathbf{e}_i \delta t, t + \delta t) - \mathbf{f}(\mathbf{x}, t) = -\Omega(\mathbf{f} - \mathbf{f}^{eq}) \tag{5}$$

where \mathbf{x} represents the particles position, t represents the real time, δt is the time step, \mathbf{f} is the vector of the discrete particle distribution functions, denoted by $\mathbf{f} = (f_0, f_1, f_2, f_3, f_4, f_5, f_6)^T$, and \mathbf{f}^{eq} is the vector of equivalent particle distribution functions, given by [28]

$$f_i^{eq} = \begin{cases} (1 - 6\gamma)T, & i = 0 \\ \gamma T, & i = 1, 2, \dots, 6 \end{cases} \tag{6}$$

where γ is a constant and $\gamma \in (0, 1/6)$. \mathbf{e}_i is the discrete velocity, expressed as

$$[\mathbf{e}_i] = [\mathbf{e}_0, \mathbf{e}_1, \mathbf{e}_2, \mathbf{e}_3, \mathbf{e}_4, \mathbf{e}_5, \mathbf{e}_6] = \begin{bmatrix} 0 & 1 & -1 & 0 & 0 & 0 & 0 \\ 0 & 0 & 0 & 1 & -1 & 0 & 0 \\ 0 & 0 & 0 & 0 & 0 & 1 & -1 \end{bmatrix} c \tag{7}$$

and Ω is the collision matrix, given by

$$\Omega = \mathbf{M}^{-1} \mathbf{S} \mathbf{M} \tag{8}$$

where \mathbf{S} is the relaxation time matrix, and \mathbf{M} is the transformation matrix. The transformation matrix \mathbf{M} and relaxation time matrix \mathbf{S} are defined as [24]

$$\mathbf{M} = \begin{bmatrix} 1, & 1, & 1, & 1, & 1, & 1, & 1 \\ 0, & 1, & -1, & 0, & 0, & 0, & 0 \\ 0, & 0, & 0, & 1, & -1, & 0, & 0 \\ 0, & 0, & 0, & 0, & 0, & 1, & -1 \\ 6, & -1, & -1, & -1, & -1, & -1, & -1 \\ 0, & 2, & 2, & -1, & -1, & -1, & -1 \\ 0, & 0, & 0, & 1, & 1, & -1, & -1 \end{bmatrix} c \tag{9}$$

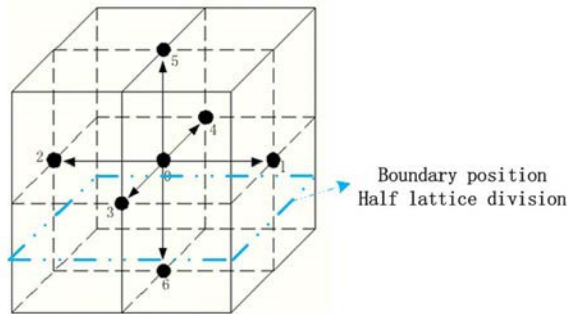


Figure 4. D3Q7 model scheme.

$$\mathbf{S}^{-1} = \begin{bmatrix} \tau_0, & 0, & 0, & 0, & 0, & 0, & 0 \\ 0, & \tau_{xx}, & \tau_{xy}, & \tau_{xz}, & 0, & 0, & 0 \\ 0, & \tau_{yx}, & \tau_{yy}, & \tau_{yz}, & 0, & 0, & 0 \\ 0, & \tau_{zx}, & \tau_{zy}, & \tau_{zz}, & 0, & 0, & 0 \\ 0, & 0, & 0, & 0, & \tau_4, & 0, & 0 \\ 0, & 0, & 0, & 0, & 0, & \tau_5, & 0 \\ 0, & 0, & 0, & 0, & 0, & 0, & \tau_6 \end{bmatrix} \quad (10)$$

The off-diagonal elements of the relaxation time matrix enable us to fully describe the anisotropic heat transfer problem. Taking components A and B as an example, the relationships between the thermal diffusivity matrices and the relaxation time coefficients are expressed as follows [29]:

$$\begin{aligned} (\tau_{ij})_A &= \frac{1}{2} \delta_{ij} + \frac{(D_{ij})_A}{\varepsilon c^2 \delta t} \quad (i = 1, 3; j = 1, 3) \\ (\tau_{ij})_B &= \frac{1}{2} \delta_{ij} + \frac{(D_{ij})_B}{\varepsilon c^2 \delta t} \quad (i = 1, 3; j = 1, 3) \end{aligned} \quad (11)$$

where δ_{ij} represents the Kronecker symbol, c represents the pseudo sound speed, ε is a constant, and $\varepsilon = 2\gamma$ if the equivalent particle distribution functions are defined by Eq. (6). In the present paper, we set γ to be $1/8$ [29]. In MRT LBM, the value of c should ensure the value of τ_{ij} between 0 and 2 [21]. The values of τ_0 , τ_4 , τ_5 , τ_6 are set to be unity without affecting the numerical accuracy [24].

As indicated above, at the interfaces between different components, the continuities of temperature and heat flux should be satisfied. If we follow the half-lattice division scheme proposed by Wang et al. [30] for LBM, the continuity condition can be easily satisfied. The accuracy of such treatment is second order, which was demonstrated in [27]. The half-lattice division scheme means placing the interface at the middle of the two lattice nodes. The local temperature and local heat flux can be calculated based on the discrete particle distribution functions if we have determined the local node to be component A or B . The local temperature is obtained by [12]

$$T = \sum_i f_i \quad (12)$$

The relationships between the first-order partial derivatives with respect to temperature and the local discrete distribution function are provided by Yoshida and Nagoka [24]:

$$\begin{aligned} -\frac{1}{\varepsilon \delta x} (f_1 - f_2) &= \tau_{xx} \frac{\partial T}{\partial x} + \tau_{xy} \frac{\partial T}{\partial y} + \tau_{xz} \frac{\partial T}{\partial z} \\ -\frac{1}{\varepsilon \delta x} (f_3 - f_4) &= \tau_{yx} \frac{\partial T}{\partial x} + \tau_{yy} \frac{\partial T}{\partial y} + \tau_{yz} \frac{\partial T}{\partial z} \\ -\frac{1}{\varepsilon \delta x} (f_5 - f_6) &= \tau_{zx} \frac{\partial T}{\partial x} + \tau_{zy} \frac{\partial T}{\partial y} + \tau_{zz} \frac{\partial T}{\partial z} \end{aligned} \quad (13)$$

By solving the above ternary linear equations, we can obtain the values of $\partial T/\partial x$, $\partial T/\partial y$, and $\partial T/\partial z$. Then, the heat fluxes along the specified directions can be calculated as follows:

$$\begin{aligned} q_x &= \rho c_p \left(D_{xx} \frac{\partial T}{\partial x} + D_{xy} \frac{\partial T}{\partial y} + D_{xz} \frac{\partial T}{\partial z} \right) \\ q_y &= \rho c_p \left(D_{yx} \frac{\partial T}{\partial x} + D_{yy} \frac{\partial T}{\partial y} + D_{yz} \frac{\partial T}{\partial z} \right) \\ q_z &= \rho c_p \left(D_{zx} \frac{\partial T}{\partial x} + D_{zy} \frac{\partial T}{\partial y} + D_{zz} \frac{\partial T}{\partial z} \right) \end{aligned} \quad (14)$$

Here, ρc_p is the volume-specific capacity. To ensure the heat flux continuity at the interface, we should set [17]

$$(\rho c_p)_A = (\rho c_p)_B \tag{15}$$

for different phases. The reason was explained in [31].

Once the temperature field is solved, the effective thermal conductivities of needed C/C-SiC composite materials along the specified directions can be obtained by

$$\begin{aligned} \lambda_{x,e} &= \frac{L_x \cdot \int q_x dA_x}{\Delta T \cdot A_x} \\ \lambda_{y,e} &= \frac{L_y \cdot \int q_y dA_y}{\Delta T \cdot A_y} \\ \lambda_{z,e} &= \frac{L_z \cdot \int q_z dA_z}{\Delta T \cdot A_z} \end{aligned} \tag{16}$$

where L_x , L_y , and L_z are the thicknesses of materials along the x , y , and z directions, respectively; and ΔT is the temperature difference between the two given boundary surfaces.

The boundary conditions of the computational domain are specified as follows. Two opposite boundary surfaces are set to be isothermal, and the other four boundary surfaces are set to be periodic other than adiabatic.

For isothermal boundary conditions, the treatment in the LBM is as follows [24]:

$$f_\alpha(t + \delta t, \mathbf{x}) = -\hat{f}_{\bar{\alpha}}(t, \mathbf{x}) + \varepsilon T_{iso} \tag{17}$$

The periodic boundary condition is set to be [12]

$$f_\alpha(t + \delta t, \mathbf{x} + L) = \hat{f}_\alpha(t, \mathbf{x}) \tag{18}$$

where \hat{f} represents the postcollision discrete temperature distribution function, the index $\bar{\alpha}$ denotes the direction opposite to α , and T_{iso} is the given temperature.

2.3. Application for needed C/C-SiC composite materials

Heat transfer in fibers has preferable directions because their thermal conductivities along the axial direction and the radial direction are different. In the needed C/C-SiC composite materials, fibers are randomly distributed in the plane of the short-cut fiber web. If the principle directions of the fiber differ from the Cartesian coordinate direction (see Figure 5), the transformation of the thermal

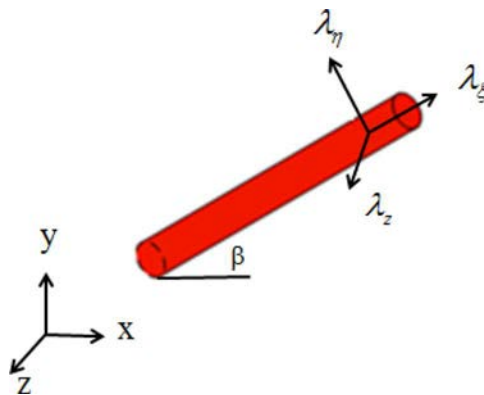


Figure 5. The random distribution of fiber in the plane.

Table 1. Thermal conductivity of constituent materials.

Constituents	Density g/cm ³	Thermal conductivity W/(m · K)	
		Transverse	Longitudinal
Fiber(T300) [32]	1.76	0.84	8.4
Carbon matrix [31]	1.80	30	30
SiC matrix [33]	3.20	70	70
Pore		0.026	0.026

conductivity matrix should be carried out as follows:

$$\lambda_{ij} = \begin{bmatrix} \lambda_{\xi} \cos^2 \beta + \lambda_{\eta} \sin^2 \beta & (\lambda_{\xi} - \lambda_{\eta}) \cos \beta \sin \beta & 0 \\ (\lambda_{\xi} - \lambda_{\eta}) \cos \beta \sin \beta & \lambda_{\xi} \sin^2 \beta + \lambda_{\eta} \cos^2 \beta & 0 \\ 0 & 0 & \lambda_z \end{bmatrix} \quad (19)$$

Here, β denotes the angle between the axial direction of fiber and the x direction, λ_{ξ} is the axial thermal conductivity of the fiber, and λ_{η} and λ_z are the two radial thermal conductivities. In the present paper, the fiber is assumed to be transversely isotropic, and thus $\lambda_{\eta} = \lambda_z$. The thermal conductivities of the constituents of the needled C/C-SiC composite materials are shown in Table 1 [32–34]. The thermal conductivity of the carbon matrix is the function of the crystallinity and processing temperature. The average thermal conductivity of carbon matrix for low crystallinity and high processing temperature situation is 30 W/(m · K) [32].

Based on the reconstructed unit cell structures, we can obtain the longitudinal and transverse effective thermal conductivities of the nonwoven cloth, short-cut fiber web, and needle fiber bundles, respectively, by using the MRT LBM developed in Section 2.2. The thermal conductivities of the needled C/C-SiC composite material are treated to be transverse isotropic and have a different value in the longitudinal direction. The longitudinal and transverse effective thermal conductivities of composite materials with no needle fiber bundles can be obtained by

$$\lambda_{e,non}^L = \frac{\lambda_c^L \lambda_w^L}{(\lambda_c^L \delta_2 + \lambda_w^L \delta_1)} (\delta_1 + \delta_2) \quad (20)$$

$$\lambda_{e,non}^T = \frac{\lambda_{c,0^\circ}^T \delta_1 / 2 + \lambda_{c,90^\circ}^T \delta_1 / 2 + \lambda_w^T \delta_2}{(\delta_1 + \delta_2)} \quad (21)$$

where δ_1 and δ_2 are the thicknesses of the nonwoven cloth and short-cut fiber web, respectively; $\lambda_{c,0^\circ}^T$, $\lambda_{c,90^\circ}^T$, and λ_w^T are the transverse thermal conductivities of the 0° nonwoven cloth, 90° nonwoven cloth, and short-cut fiber web, respectively; and λ_c^L and λ_w^L are the longitudinal thermal conductivities of the nonwoven cloth and short-cut fiber web, respectively.

The longitudinal thermal conductivity of the needled C/C-SiC composite material then can be calculated by

$$\lambda_e^L = \lambda_{e,non}^L (1 - \phi_n) + \lambda_n^L \phi_n \quad (22)$$

where ϕ_n is the volume fraction of the needle fiber bundle, and λ_n^L is the thermal conductivity of the needle fiber bundle. The influence of the needle fiber bundle on the transverse thermal conductivity of the needled C/C-SiC composite materials can be neglected.

3. Experimental measurement

To validate the reasonableness and accuracy of the model and method proposed in the present paper, some corresponding experimental measurements were conducted. The test materials were prepared by the Northwestern Polytechnical University (NPU), Xi'an, China. The volume fraction of carbon

Table 2. Information of materials.

	Density g/cm ³	Porosity %	Carbon matrix %	Carbon fiber %	SiC matrix %
Material 1	1.946	12	33	28	27
Material 2	1.647	25	25	28	22

fiber depends on the preform of the composite materials, and it is 28%. We assume that the phase Si does not exist in the composite materials. The mass content of carbon and SiC can be determined by gravimetric analysis. If the densities of the carbon fiber, carbon matrix, and SiC matrix are obtained, we can obtain the volume fraction of each constituent. The volume fractions of the porosity, carbon matrix, carbon fiber (T300), and SiC matrix of the two different needed C/C-SiC composite materials are shown in Table 2. The fiber volume fraction of the nonwoven cloth is 78.5% because the fibers are compactly arranged with no gap. The mass ratio of the fiber in the nonwoven cloth and that in the short-cut fiber web is 0.85:0.15. The thickness of the nonwoven cloth is 0.404 mm, and the thickness of the short-cut fiber web is 0.929 mm.

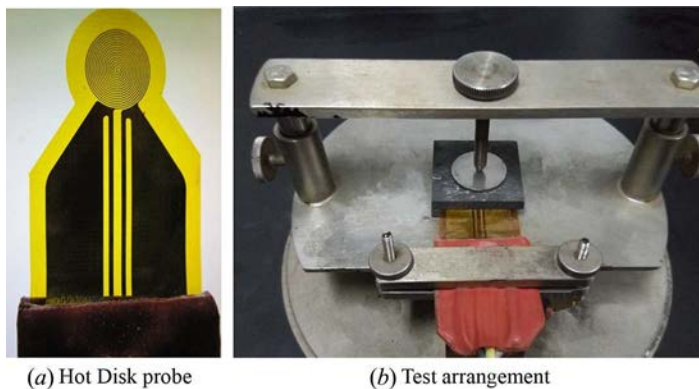
The Hot Disk thermal constants analyzer can measure the heat capacity of the materials [35], and it can be applied to determine the longitudinal and transverse thermal conductivities of the anisotropic materials [25]. During the measurement of the thermal conductivity, the Hot Disk probe is put between the two identical samples (see Figure 6). The Hot Disk thermal constants analyzer supplies a certain power to the probe during the measuring time. The surface of the sample facing the probe then has a temperature increase, and it depends on the thermal property of the materials. The expression of the temperature increase is shown as follows [25]:

$$\Delta T_s(\tau_T) = \frac{P_0}{\pi^{3/2} r (\lambda_T \lambda_L)^{1/2}} D(\tau_T) \quad (23)$$

where P_0 is the input power, r is the radius of the probe, λ_T and λ_L are the transverse and longitudinal effective thermal conductivities of the specimen, respectively, $D(\tau_T)$ is the dimensionless specific time function, and τ_T is defined as

$$\tau_T = \sqrt{a_T t} / r \quad (24)$$

where a_T is the transverse thermal diffusivity of the materials, and t is the measurement time. The linear relationship of $\Delta T_s(\tau_T)$ and $D(\tau_T)$ is established through an iteration procedure with transverse thermal diffusivity as the optimization variable. The transverse thermal diffusivity of materials is determined from the final step of the iteration procedure [25]. If the volume capacity of the materials

**Figure 6.** Hot Disk probe and gold container.

is known, the transverse thermal conductivity of the material is

$$\lambda_T = \rho c_p \cdot a_T \quad (25)$$

The longitudinal thermal conductivity of the specimen, λ_L , can then be determined through the slope of the line presented in Eq. (23).

On the heat capacity measurement via the Hot Disk method, reference [35] can be consulted.

4. Results and discussion

The measured volume capacities of materials 1 and 2 are $1.28 \text{ MJ}/(\text{m}^3 \cdot \text{K})$ and $1.02 \text{ MJ}/(\text{m}^3 \cdot \text{K})$, respectively. The comparisons of the experimental data and the numerical predictions of the effective thermal conductivities are shown in Table 3. λ_T and λ_L are the measured transverse and longitudinal thermal conductivities, respectively; λ_e^T and λ_e^L are the numerical prediction results. It can be seen that the transverse thermal conductivity of the composite material is larger than the longitudinal thermal conductivity. The numerical predictions of the longitudinal and transverse thermal conductivities of the composite materials agree well with the experimental data, and the maximum deviation is 11.36%. Thus, the present model and the numerical method can be adopted to predict the longitudinal and transverse thermal conductivities of the composite materials and to determine the factors that affect the longitudinal and transverse thermal conductivities of the needled C/C-SiC composite materials.

4.1. Effect of the needle fiber bundle

The fibers in the needle fiber bundle consist of the fibers from the nonwoven cloth and short-cut fiber web. Therefore, we assume that the fiber volume fraction of the needle fiber bundle is the same as the total fiber volume fraction of the composite materials. Thus, the fiber volume fraction of the needle fiber bundle is set to be 28%. The average diameter of the needle fiber bundle is 0.2 mm. The needling density is averagely 36 needle fiber bundles per square centimeter. The effect of the needle fiber bundle on the longitudinal thermal conductivity of the needled C/C-SiC composite materials is shown in Figure 7. It can be seen that in the low-porosity region, the needle fiber bundle can enhance the longitudinal thermal conductivity of the composite materials. However, the enhancement effect of the needle fiber bundle is not significant and decreases when the porosity of the composite materials increases. The main purpose of needling the composite materials is to improve the interlaminar shear strength.

4.2. Effect of porosity

The effect of porosity on the longitudinal and transverse thermal conductivity of needled C/C-SiC composite materials is investigated. Figure 8 shows the variations of the longitudinal and transverse thermal conductivities of the needled C/C-SiC composite materials with porosity. It can be seen that the longitudinal thermal conductivity is larger than the transverse thermal conductivity of the composite materials. The constituents of the needled C/C-SiC composite materials are carbon fibers, carbon matrices, SiC matrices, and pores. The volume fractions of fibers and carbon matrices are given as 28% and 20%, respectively. Thus, a larger porosity results in a smaller SiC matrix volume

Table 3. Comparisons of the experimental data and the numerical predictions.

	$\lambda_T^{(\text{Exp})}$ W/(m · K)	λ_e^T W/(m · K)	Deviation %	$\lambda_L^{(\text{Exp})}$ W/(m · K)	λ_e^L W/(m · K)	Deviation %
Material 1	18.21	19.87	9.11	7.12	7.51	5.47
Material 2	10.70	11.48	7.28	5.06	5.75	11.36

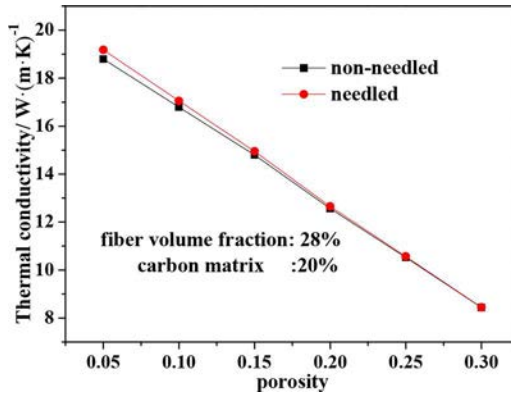


Figure 7. Effect of the needle fiber bundle on the longitudinal thermal conductivity.

fraction. When the porosity increases, both the longitudinal and transverse thermal conductivities of the materials decrease due to the thermal conductivity of the SiC being larger than that of gas in pores.

4.3. Effect of the carbon matrix content

The effect of the carbon matrix volume fraction on the longitudinal and transverse thermal conductivities of the needled C/C-SiC composite materials is shown in Figure 9. The fiber volume fraction and porosity of the composite materials are set to be typical values as 28% and 12%, respectively. A larger carbon matrix volume fraction results in a smaller SiC matrix volume fraction. When the volume fraction of the carbon matrix increases, both the longitudinal and transverse thermal conductivities of the composite materials decrease because the thermal conductivity of the SiC matrix is larger than that of the carbon matrix.

4.4. Effect of the fiber volume fraction

The effect of fiber volume fraction on the longitudinal and transverse thermal conductivities of the needled C/C-SiC composite materials is shown in Figure 10. Figure 10a shows the variations of the longitudinal and transverse thermal conductivities of the needled C/C-SiC composite materials with the fiber volume fraction of the composite materials. The carbon matrix volume fraction and

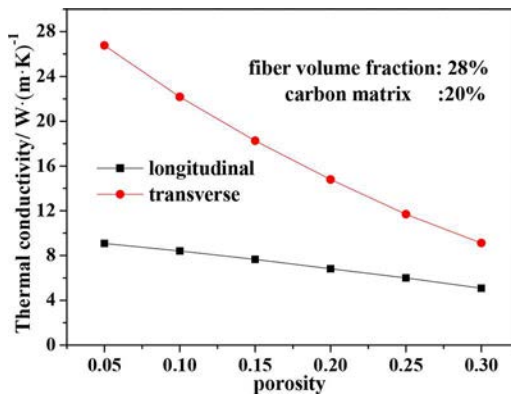


Figure 8. Effect of porosity on thermal conductivity.

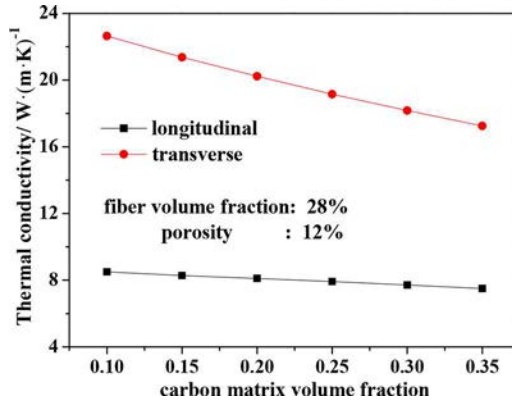
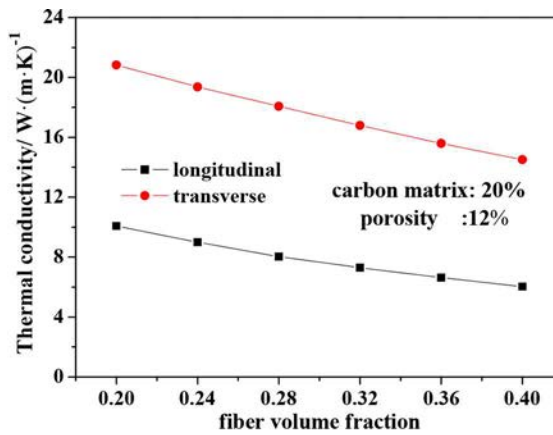
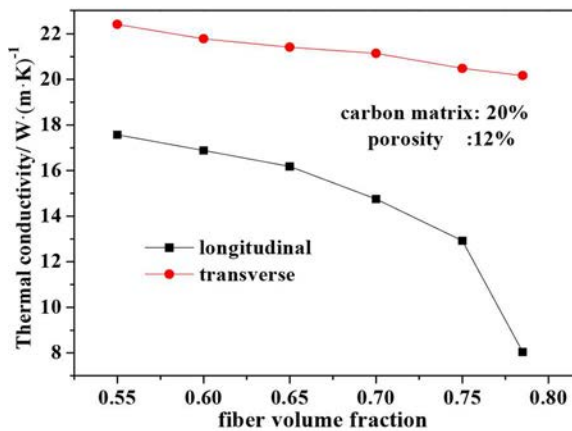


Figure 9. Effect of the carbon matrix content on thermal conductivity.

porosity of the composite materials are given as 20% and 12%, respectively. A larger fiber volume fraction results in a smaller SiC matrix volume fraction. When the fiber volume fraction increases, both the longitudinal and transverse thermal conductivities of the composite materials decrease because of its smaller thermal conductivity.



(a) Total fiber volume fraction of composite material



(b) Fiber volume fraction of non-woven cloth

Figure 10. Effect of the fiber volume fraction on thermal conductivity.

The transverse thermal conductivity of the needled C/C-SiC composite materials is larger than the longitudinal thermal conductivity due to the anisotropic property of the nonwoven cloth. In the nonwoven cloth, fibers are unidirectional and arranged compactly (fiber volume fraction being 0.785) to enhance the strength, and fibers are the major conductive medium of the nonwoven cloth. The axial thermal conductivity (along the transverse direction) of fibers is much larger than the radial thermal conductivity (as low as $0.84 \text{ W}/(\text{m} \cdot \text{K})$ along the longitudinal direction), resulting in the larger transverse thermal conductivity of the nonwoven cloth than its longitudinal thermal conductivity. Thus, in the longitudinal direction the layer of the nonwoven cloth is the main thermal resistance of the needled C/C-SiC composite materials. [Figure 10b](#) shows the variations of the longitudinal and transverse thermal conductivities with the fiber volume fraction of the nonwoven cloth. The total fiber volume fractions of the composite material, carbon matrix, and porosity are given as 28%, 20%, and 12%, respectively. It can be seen that the transverse thermal conductivities increase while the longitudinal thermal conductivities remain almost unchanged when the fiber volume fraction of the nonwoven cloth decreases. At the highest fiber volume fraction, a decrease in the fiber volume fraction of the nonwoven cloth leads to a drastic increase in the longitudinal thermal conductivity of the needled C/C-SiC composite materials. It is because when the fiber volume fraction of the nonwoven cloth is smaller than the value of 0.785, the fiber is surrounded with the dual matrix and does not come in contact with another fiber, leading to the drastic increase in the longitudinal thermal conductivity of the nonwoven cloth.

4.5. Effect of the high thermal conductivity of fibers

In Section 4.4, we have mentioned that the layer of nonwoven cloth is the main thermal resistance of needled C/C-SiC composite materials in the longitudinal direction. Therefore, the thermal conductivity of the carbon fiber is an important parameter that controls the longitudinal thermal conductivity of needled C/C-SiC composite materials. [Figures 11a](#) and [b](#) show the effect of the high thermal conductivity fiber on the longitudinal and transverse thermal conductivities. The axial thermal conductivity of the high thermal conductivity fiber is $40 \text{ W}/(\text{m} \cdot \text{K})$, and the radial thermal conductivity of the high thermal conductivity fiber is $4 \text{ W}/(\text{m} \cdot \text{K})$. It can be seen that both longitudinal and transverse thermal conductivities of the needled C/C-SiC composite materials with the high thermal conductivity fiber are enhanced compared with those with the T300 carbon fiber. The enhancement effect of the longitudinal thermal conductivity is more significant than the transverse thermal conductivity. If the needled C/C-SiC composite materials serve as braking materials, a larger thermal conductivity of the composite materials is better because the heat generated due to the friction will be easy to be taken away.

4.6. Effect of the thermal contact resistance

From the comparisons of the experimental data and the numerical predictions of the needled C/C-SiC composite materials shown in [Table 3](#), we can see that the numerical predictions are a little larger than the experimental data. For the short-cut fiber web in needled C/C-SiC composite materials, the thermal contact resistance between fibers and matrices cannot be ignored, resulting in the deviations between the numerical results and the experimental data. To consider the thermal contact resistance, we simply embed the thermal contact resistance into the microstructure of the composite materials. The surface of the fibers is covered by a thin layer with its local thermal conductivities lower than the matrices to consider the thermal contact resistance between the fibers and matrices. The influence of the internal thermal contact resistance on the composite materials is shown in [Figure 12](#). It can be seen that the effective thermal conductivity of the needled C/C-SiC composite materials decreases when the thermal contact resistance increases. The predicted effective thermal conductivity with thermal contact resistance being $2 \times 10^{-6} \text{ m}^2 \cdot \text{K}/\text{W}$ has a better agreement with the experimental data than those ignoring the thermal contact resistance.

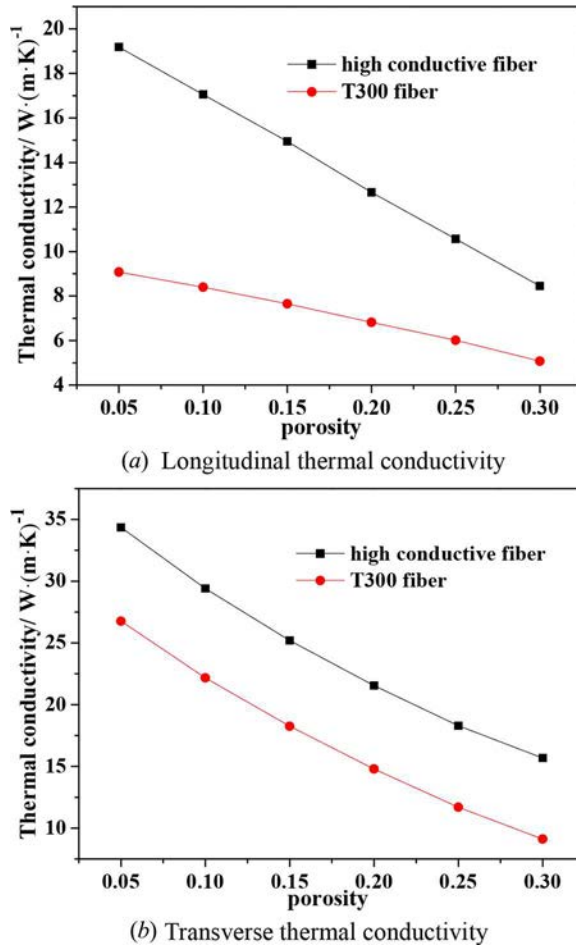


Figure 11. Effect of the high thermal conductivity fiber on the thermal conductivity of composite materials.

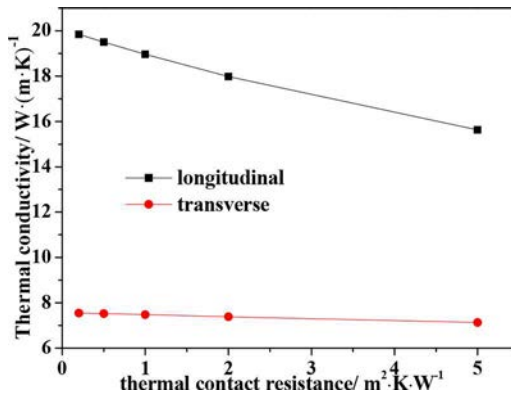


Figure 12. The influence of the thermal contact resistance on the effective thermal conductivity.

5. Conclusion

In the present paper, the complicated structures of needled C/C-SiC composite materials with random distributions of fibers and pores are reconstructed. Then, an MRT LBM is developed to predict the transverse and longitudinal thermal conductivities of the needled C/C-SiC composite materials whose constituents are anisotropic. The accuracy is verified by the experimental data conducted by the Hot Disk analyzer. After validations, the factors that affect the longitudinal and transverse thermal conductivities of the needle C/C-SiC composite materials are investigated. The following conclusions can be drawn:

1. The MRT LB model with off-diagonal elements in the relaxation time matrix can be adopted to numerically predict the longitudinal and transverse thermal conductivities of the needled C/C-SiC composite materials based on the reconstructed unit cell structures;
2. The transverse thermal conductivity of the required C/C-SiC composite materials is larger than its longitudinal thermal conductivity; both longitudinal and transverse thermal conductivities decrease when the porosity, carbon matrix contents, fiber volume fractions of composite materials, and fiber volume fraction of the nonwoven cloth increase; using high thermal conductive fibers can significantly improve the longitudinal thermal conductivity of the needled C/C-SiC composite materials; a larger thermal contact resistance will lead to a smaller effective thermal conductivity.

Funding

This work was supported by the Key Project of International Joint Research of National Natural Science Foundation of China (51320105004) and the 111 Project (B16038).

References

- [1] W. Krenkel, Carbon Fiber Reinforced CMC for High-Performance Structures, *Int. J. Appl. Ceram. Tec.*, vol. 1, pp. 188–200, 2001.
- [2] W. Krenkel and F. Berndt, C/C-SiC Composites for Space Applications and Advanced Friction Systems, *Mater. Sci. Eng. A - Struct.*, vol. 412, pp. 177–181, 2005.
- [3] Y. D. Xu, L. F. Cheng, and L. T. Zhang, Carbon/Silicon Carbide Composites Prepared by Chemical Vapor Infiltration Combined with Silicon Melt Infiltration, *Carbon*, vol. 37, pp. 1179–1187, 1999.
- [4] J. Nie, Y. D. Xu, L. T. Zhang, L. F. Cheng, and J. Ma, Microstructure and Tensile Behavior of Multiply Needled C/SiC Composite Fabricated by Chemical Vapor Infiltration, *J. Mater. Process Tech.*, vol. 209, pp. 572–576, 2009.
- [5] Y. Cai, Y. D. Xu, B. Li, S. Fan, L. T. Zhang, L. F. Cheng, and L. Yu, Low-Cost Preparation and Frictional Behaviour of a Three-Dimensional Needled Carbon/Silicon Carbide Composite, *J. Eur. Ceram. Soc.*, vol. 29, pp. 497–503, 2009.
- [6] P. Xiao, Z. Li, and X. Xiong, Microstructure and Tribological Properties of 3D Needle-Punched C/C-SiC Brake Composites, *Solid State Sci.*, vol. 12, pp. 617–623, 2010.
- [7] S. Fan, Y. D. Xu, L. T. Zhang, L. F. Cheng, L. Yu, Y. Yuan, F. Zhang, G. Tian, Z. Chen, and J. Lou, Three-dimensional Needled Carbon/Silicon Carbide Composites with High Friction Performance, *Mater. Sci. Eng. A - Struct.*, vol. 467, pp. 53–58, 2007.
- [8] Y. Cai, Y. D. Xu, B. Li, S. Fan, L. T. Zhang, L. F. Cheng, B. Dong, and J. Jiang, Microstructures and Mechanical Properties of a Low-Cost Three-dimensional Needled Carbon/Silicon Carbide Composite, *Mater. Sci. Eng. A - Struct.*, vol. 497, pp. 278–282, 2008.
- [9] J. Chen, Y. Wang, L. F. Cheng, and L. T. Zhang, Thermal Diffusivity of Three-Dimensional Needled C/SiC-TaC Composites, *Ceram. Int.*, vol. 37, pp. 3095–3099, 2011.
- [10] L. F. Cheng, Y. D. Xu, Q. Zhang, and L. T. Zhang, Thermal Diffusivity of 3D C/SiC Composites from Room Temperature to 1400°C, *Carbon*, vol. 41, pp. 707–711, 2003.
- [11] D. S. Li, D. N. Fang, and N. Jiang, Finite Element Modeling of Mechanical Properties of 3D Five-Directional Rectangular Braided Composites, *Compos. Part B - Eng.*, vol. 42, pp. 1373–1385, 2011.
- [12] A. Tarokh, A. A. Mohamad, and L. Jiang, Simulation of Conjugate Heat Transfer Using the Lattice Boltzmann Method, *Numer. Heat. Transfer A - Appl.*, vol. 63, pp. 159–178, 2013.
- [13] L. Chen, H. B. Luan, Y. L. He, Pore-Scale Flow and Mass Transport in Gas Diffusion Layer of Proton Exchange Membrane Fuel Cell with Interdigitated Flow Fields[J], *Int. J. Therm. Sci.*, vol. 51, pp. 132–144, 2012.

- [14] G. Imani, M. Maerefat, and K. Hooman, Lattice Boltzmann Simulation of Conjugate Heat Transfer from Multiple Heated Obstacles Mounted in a Walled Parallel Plate Channel, *Numer. Heat Transfer A - Appl.*, vol. 62, pp. 798–821, 2012.
- [15] W. Q. Tao, *Numerical Heat Transfer*, Xi'an Jiaotong University Press, Xi'an, 2001.
- [16] H. B. Luan, H. Xu, L. Chen, D. L. Sun, Y. L. He, and W. Q. Tao, Evaluation of the Coupling Scheme of FVM and LBM for Fluid Flows Around Complex Geometries, *Int. J. Heat Mass Trans.*, vol. 54, pp. 1975–1985, 2011.
- [17] M. Wang, J. Wang, N. Pan, and S. Chen, Mesoscopic Predictions of the Effective Thermal Conductivity for Microscale Random Porous Media, *Phys. Rev. E.*, vol. 75, pp. 036702, 2007.
- [18] M. Wang and N. Pan, Modeling and Prediction of the Effective Thermal Conductivity of Random Open-Cell Porous Foams, *Int. J. Heat Mass Transfer*, vol. 51, pp. 1325–1331, 2008.
- [19] M. Wang, J. He, J. Yu, and N. Pan, Lattice Boltzmann Modeling of the Effective Thermal Conductivity for Fibrous Materials, *Int. J. Therm. Sci.*, pp. 848–855, 2007.
- [20] Y. Qian, D. d'Humières and P. Lallemand, Lattice BGK Models for Navier-Stokes Equation, *EPL-Europhys. Lett.*, vol. 17, pp. 479, 1992.
- [21] D. d'Humières, Multiple-Relaxation-Time Lattice Boltzmann Models in Three Dimensions, *P. Roy. Soc. A - Math. Phys.*, vol. 360, pp. 437–451, 2002.
- [22] L. Li, R. Mei, and J. F. Klausner, Multiple-Relaxation-Time Lattice Boltzmann Model for the Axisymmetric Convection Diffusion Equation, *Int. J. Heat Mass Transfer*, vol. 67, pp. 338–351, 2013.
- [23] I. Rasin, S. Succi, and W. Miller, A Multi-Relaxation Lattice Kinetic Method for Passive Scalar Diffusion, *J. Comput. Phys.*, vol. 206, pp. 453–462, 2005.
- [24] H. Yoshida and M. Nagaoka, Multiple-Relaxation-Time Lattice Boltzmann Model for the Convection and Anisotropic Diffusion Equation, *J. Comput. Phys.*, vol. 229, pp. 7774–7795, 2010.
- [25] ISO22007–2 (2008). Plastics: Determination of Thermal Source (hot disc) Method.
- [26] <http://www.toraycfa.com/pdfs/T300DataSheet.pdf>
- [27] L. Li, C. Chen, R. Mei, and J. F. Klausner, Conjugate Heat and Mass Transfer in the Lattice Boltzmann Equation Method, *Phys. Rev. E*, vol. 89, pp. 043308, 2014.
- [28] H. Yoshida, T. Kobayashi, H. Hayashi, T. Kinjo, H. Washizu, and K. Fukuzawa, Boundary Condition at a Two-phase Interface in the Lattice Boltzmann Method for the Convection-diffusion Equation, *Phys. Rev. E*, vol. 90, pp. 013303, 2014.
- [29] L. Li, R. Mei, and J. F. Klausner, Boundary Conditions for Thermal Lattice Boltzmann Equation Method, *J. Comput. Phys.*, vol. 237, pp. 366–395, 2013.
- [30] J. Wang, M. Wang, and Z. Li, A Lattice Boltzmann Algorithm for Fluid–Solid Conjugate Heat Transfer, *Int. J. Therm. Sci.*, vol. 46, pp. 228–234, 2007.
- [31] W. Z. Fang, J. J. Gou, H. Zhang, L. Chen, and W. Q. Tao, Numerical Predictions of Effective Thermal Conductivities for Three-Dimensional Four-directional Braided Composites Using the Lattice Boltzmann Method, *Int. J. Heat Mass Transfer*, vol. 92, pp. 120–130, 2016.
- [32] P. D. Puglia, M. A. Sheikh, and D. R. Hayhurst, Modelling the Degradation of Thermal Transport in a CMC Material due to Three Different Classes of Porosity, *Model. Simul. Mater. Sci.*, vol. 12, pp. 357–372, 2004.
- [33] Q. G. Ning and T. W. Chou, A Closed-form Solution of the Transverse Effective Thermal Conductivity of Woven Fabric Composites, *J. Compos. Mater.*, vol. 29, pp. 2280–2294, 1995.
- [34] J. K. Farooqi and M. A. Sheikh, Finite Element Modelling of Thermal Transport in Ceramic Matrix Composites, *Comp. Mater. Sci.*, vol. 37, pp. 361–373, 2006.
- [35] A. Berge, B. A. Zarrabi, and C. E. Hagentoft, Determination of Specific Heat Capacity by Transient Plane Source, *Fron. Archit. Res.*, vol. 2, pp. 476–482, 2013.